Acta Mech 202, 79–99 (2009)
DOI 10.1007/s00707-008-0037-3

R. H. Plaut

Linearly elastic annular and circular membranes under radial, transverse, and torsional loading. Part I: large unwrinkled axisymmetric deformations

Received: 25 January 2008 / Published online: 10 June 2008

Abstract Three theories for determination of the equilibrium states of initially flat, linearly elastic, rotationally symmetric, taut membranes are considered: Föppl-von Kármán theory, Reissner's theory, and a new generalization of Reissner's theory that does not restrict the strains to be small. Attention is focused on annular membranes, but circular membranes are also treated. Large deformations are allowed, and the equilibrium equations are written in terms of transverse, radial, and circumferential displacements. Problems considered include radial stretching, transverse displacement of the inner edge, an adhesive punch pull-off test on a circular blister, transverse pressure, ponding of annular and circular membranes, a vertical distributed load with a vertically sliding outer membrane edge, pull-in (snap-down, jump-to-contact) instability of a MEMS device, torsion of the inner or outer edge of a stretched membrane, and a combination of radial stretching, vertical displacement, and torsion. Results for the three theories are compared. Closed-form solutions are available in a few cases, but usually a shooting method is utilized to obtain numerical solutions for displacements, strains, and stresses. Conditions for the onset of wrinkling are determined. In the second part of this two-part study, small vibrations about equilibrium configurations are analyzed.

1 Introduction

Membrane structures and structural components are of much interest in a variety of applications [1–3]. They often exhibit large deflections. Since they cannot resist compression, they are susceptible to wrinkling. Linearly elastic annular membranes and some circular membranes are considered in this paper. They are initially flat (horizontal). The loading is rotationally symmetric, and the membranes are taut (i.e., not wrinkled or slack).

Nonlinear static analyses are presented in terms of radial, meridional, and circumferential displacements. Three theories are utilized. One is Föppl-von Kármán theory [1,2,4] (to be denoted the FvK theory), another is Reissner's theory [5] (to be called the R theory), and in addition a generalization of Reissner's theory is introduced (to be labeled the GR theory) in which the strains are not restricted to be negligible compared to unity. Displacements, strains, stress resultants, and conditions for wrinkling are determined. Closed-form solutions are available in a few cases. In the other cases, a shooting method is applied to obtain numerical solutions, using the programs NDSolve and FindRoot in Mathematica [6].

In the following section, the equilibrium equations in terms of displacements are derived for the three theories for torsionless loading conditions. In Sect. 3, the annular membrane is stretched radially, either by pulling inward at its inner edge or by pulling outward at its outer edge. The resulting radial tension is not constant. In Sect. 4.1, the inner edge is displaced downward, either with or without inward radial stretching. A closed-form solution for an adhesive problem is derived in Sect. 4.2, where a rigid, flat, circular punch is

R. H. Plaut (✉)
Department of Civil and Environmental Engineering, Virginia Polytechnic Institute and State University,
Blacksburg, VA 24061, USA
E-mail: rplaut@vt.edu

adhered to a circular membrane and is pulled transversely until the membrane separates when the contact radius reduces to a certain threshold value.

Transverse pressure is applied in Sect. 5. An annular membrane is considered first. Next, a circular membrane is deformed by pressure until it contacts a rigid horizontal surface; this problem is related to the constrained blister test for adhesion. The classic problem of a circular membrane subjected to pressure is also treated. In Sect. 6, full ponding of annular and circular membranes is investigated, in which the membrane holds a liquid whose top surface is at the level of the membrane's supporting edge or edges. In Sect. 7, a distributed vertical load is applied and the outer edge of the annular membrane is allowed to slide vertically (but is constrained against radial displacement and rotation). This problem is motivated by an application of geosynthetic reinforcement in geotechnical engineering.

An example from the field of microelectromechanical systems (MEMS) is analyzed in Sect. 8. An electrostatic force from a rigid plate pulls a circular or annular membrane downward until it becomes unstable and jumps into contact with the plate. In Sects. 9 and 10, the inner edge of an outwardly stretched, annular membrane is subjected to torsion, and the FvK theory is used in the analysis. A transverse displacement of the inner edge is also applied in Sect. 10.

Concluding remarks are presented in Sect. 11. In Part II of this study [7], small vibrations (axisymmetric and non-axisymmetric) about equilibrium configurations are investigated with the FvK theory for some of the problems treated below.

2 Equilibrium formulation

It is assumed in Sects. 2–8 that the circumferential displacement $V(R)$ is zero (i.e., there is no torsion), and that the radial and transverse displacements are rotationally symmetric. It is assumed that the membrane is taut. The onset of wrinkling is determined by the condition that the minimum principal stress resultant reduces to zero [8]. The self-weight of the membrane is neglected in the equilibrium analyses.

2.1 Generalized Reissner (GR) theory

A cross section along a radius of the membrane is depicted in Fig. 1. The membrane is assumed to be isotropic, homogeneous, and linearly elastic with modulus of elasticity E, Poisson's ratio ν, and constant thickness h. It is subjected to a distributed load with tangential and normal components P_t and P_n per unit of deformed area, respectively. The radial coordinate is R, with $A \le R \le B$. The radial displacement is $U(R)$, the downward displacement is $W(R)$, and the meridional rotation is $\phi(R)$. The circumferential coordinate is θ.

For an incremental change in arc length in Fig. 1, the horizontal projection is $\mathrm{d}R + \mathrm{d}U$ and the vertical projection is $\mathrm{d}W$. Hence [9]

$$W' = (1 + U')\tan\phi. \tag{1}$$

The arc length of an element in the deflected membrane is $[\alpha_r^2 \mathrm{d}R^2 + \alpha_\theta^2 \mathrm{d}\theta^2]^{1/2}$, where [5,10]

$$\alpha_r = [(1 + U')^2 + (W')^2]^{1/2} = 1 + \varepsilon_r, \quad \alpha_\theta = R + U = R(1 + \varepsilon_\theta). \tag{2a,b}$$

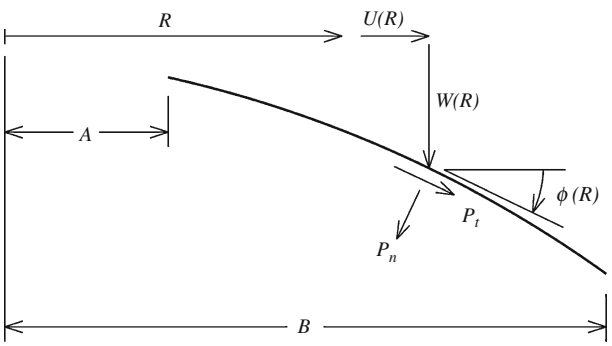

Fig. 1 Cross section along membrane radius in dimensional terms

Using Eqs. (1) and (2), the meridional and circumferential strains may be written as

$$\varepsilon_r = [(1 + U')/\cos\phi] - 1, \quad \varepsilon_\theta = U/R. \tag{3a,b}$$

The use of the rotation ϕ in Eqs. (3) instead of the square root in Eq. (2a) is convenient.

The radial and circumferential stress resultants are $N_r(R)$ and $N_\theta(R)$, respectively. The tangential and normal equilibrium equations are [5]

$$(\alpha_\theta N_r)' - \alpha_\theta' N_\theta = -\alpha_r \alpha_\theta P_t, \quad (N_r/R_r) + (N_\theta/R_\theta) = -P_n, \tag{4a,b}$$

where

$$1/R_r = \phi'/\alpha_r = \phi' \cos\phi/(1 + U'), \quad 1/R_\theta = W'/(\alpha_r \alpha_\theta) = (\sin\phi)/(R + U). \tag{5a,b}$$

Linear stress–strain relationships are assumed. Since the engineering strains are used in Eqs. (3), and the stress resultants in Eqs. (4) are defined with respect to the deformed configuration, the following relationships are assumed, with factors $1 + \varepsilon_\theta$ and $1 + \varepsilon_r$ in the respective denominators [11,12]:

$$N_r = Eh(\varepsilon_r + \nu\varepsilon_\theta)/[(1 - \nu^2)(1 + \varepsilon_\theta)], \quad N_\theta = Eh(\varepsilon_\theta + \nu\varepsilon_r)/[(1 - \nu^2)(1 + \varepsilon_r)]. \tag{6a,b}$$

The analysis is conducted in terms of nondimensional quantities:

$$\begin{aligned} r = R/B, \quad a = A/B, \quad u = U/B, \quad w = W/B, \quad n_r = N_r/(Eh), \\ n_\theta = N_\theta/(Eh), \quad p_t = P_t B/(Eh), \quad p_n = P_n B/(Eh). \end{aligned} \tag{7}$$

With the use of Eqs. (2), (3) and (5)–(7), Eq. (1) becomes

$$w' = (1 + u')\tan\phi \tag{8}$$

and Eqs. (4) can be written in the form

$$\begin{aligned} &(\nu r - u)\cos^3\phi - (1 + \nu)r\cos^2\phi + r(1 + u' + ru'')\cos\phi + r^2(1 + u')\phi'\sin\phi \\ &\quad = -(1 - \nu^2)(1 + u')(r + u)(r\cos\phi)p_t \end{aligned} \tag{9}$$

and

$$r(r\phi' + \nu\sin\phi)(1 + u' - \cos\phi) + (\nu r\phi' + \sin\phi)u\cos\phi = -(1 - \nu^2)(1 + u')(r + u)rp_n, \tag{10}$$

where primes denote differentiation with respect to r. After appropriate boundary conditions are defined at the inner edge $r = a$ and the outer edge $r = 1$, Eqs. (8)–(10) can be solved numerically for $w(r)$, $u(r)$, and $\phi(r)$.

In terms of displacements, the stress resultants are

$$\begin{aligned} n_r &= [(1 + u' - \cos\phi)r + \nu u\cos\phi]/[(1 - \nu^2)(r + u)\cos\phi], \\ n_\theta &= [u\cos\phi + \nu r(1 + u' - \cos\phi)]/[(1 - \nu^2)(1 + u')r]. \end{aligned} \tag{11a,b}$$

Even though this GR theory does not require that the strains are small, it assumes that the material behavior is linearly elastic, and this constitutive law often is not applicable for large strains. Almost all the numerical results presented here will involve strains smaller than 0.05.

2.2 Reissner (R) theory

In the theory developed by Reissner [5], it is assumed that the strains are small, i.e., that ε_r and ε_θ are negligible compared to unity. From Eqs. (2), (3), (5) and (6), the following equations are used:

$$\alpha_r \approx 1, \quad \alpha_\theta = R(1+\varepsilon_\theta) \approx R, \quad \alpha_\theta' = 1 + U' = (1+\varepsilon_r)\cos\phi \approx \cos\phi, \quad 1/R_r \approx \phi', \quad 1/R_\theta \approx (\sin\phi)/R. \tag{12}$$

Also,

$$N_r = Eh(\varepsilon_r + \nu\varepsilon_\theta)/(1-\nu^2), \quad N_\theta = Eh(\varepsilon_\theta + \nu\varepsilon_r)/(1-\nu^2), \tag{13a,b}$$

where the strains are given by Eqs. (3). With the application of Eqs. (12) and (13), the remaining equations in Eqs. (1)–(7) lead to the following equations for the nondimensional displacements $u(r)$ and $\phi(r)$:

$$\begin{aligned}&(\nu r - u)\cos^3\phi - (1+\nu)r\cos^2\phi + r(1+u'+ru'')\cos\phi + r^2(1+u')\phi'\sin\phi \\ &\quad = -(1-\nu^2)r^2 p_t \cos^2\phi\end{aligned} \tag{14}$$

and

$$r(r\phi' + \nu\sin\phi)(1+u'-\cos\phi) + (\nu r\phi' + \sin\phi)u\cos\phi = -(1-\nu^2)r^2 p_n \cos\phi. \tag{15}$$

Also, Eq. (8) is valid.

The stress resultants in terms of displacements are given by

$$\begin{aligned}n_r &= [(1+u'-\cos\phi)r + \nu u\cos\phi]/[(1-\nu^2)r\cos\phi], \\ n_\theta &= [u\cos\phi + \nu r(1+u'-\cos\phi)]/[(1-\nu^2)r\cos\phi].\end{aligned} \tag{16a,b}$$

As written, the left-hand sides of Eqs. (9) and (14) are the same, and the left-hand sides of Eqs. (10) and (15) are the same. Therefore the displacements (and strains) for the R and GR theories are the same if the right-hand sides of those equations are respectively the same. This will occur in Sects. 3 and 4 where $p_t = p_n = 0$. It also will occur in Sect. 7 where a vertical distributed load is constant per unit of undeformed area of the horizontal projection of the membrane, and in Sect. 8 for the MEMS example. However, the stress resultants in these cases are not the same for the R and GR theories.

2.3 Föppl-von Kármán (FvK) theory

The FvK equations do not involve the rotation $\phi(R)$. Consider rotationally symmetric equilibrium in terms of $U(R)$ and $W(R)$. As in the R theory, ε_r and ε_θ are assumed to be negligible compared to unity, with ε_θ given in Eq. (3b) and ε_r given in the FvK theory by

$$\varepsilon_r = U' + 0.5(W')^2. \tag{17}$$

Expansion of Eq. (2a) can be written as

$$\varepsilon_r = U' + 0.5(W')^2[1 - U' + (U')^2 - (U')^3 - 0.25(W')^2 + 0.75U'(W')^2] + \ldots \tag{18}$$

and as

$$\begin{aligned}\varepsilon_r = {} & U'[1 - 0.5(W')^2 + 0.5U'(W')^2 + 0.375(W')^4 - 0.5(U')^2(W')^2] \\ & + 0.5(W')^2[1 - 0.25(W')^2] + \ldots\end{aligned} \tag{19}$$

Therefore the quantities in brackets in Eqs. (18) and (19) are replaced by unity to give Eq. (17), and hence it is assumed here that U/R, U', and $(W')^2$ are small compared with unity. (Similar restrictions also apply in the R theory, since the strains are neglected in comparison with unity, and hence the rotations ϕ are restricted.)

With the use of Eqs. (3b), (4), (7), (13), (17), and

$$\alpha_r \approx 1, \quad \alpha_\theta \approx R, \quad \alpha_\theta' \approx 1, \quad 1/R_r \approx W', \quad 1/R_\theta \approx W'/R, \tag{20}$$

one obtains the following nondimensional equations for equilibrium in the radial and vertical directions [13–15]:

$$r^2u'' + ru' - u + r^2w'w'' + 0.5(1-\nu)r(w')^2 = -(1-\nu^2)r^2p_t \tag{21}$$

and

$$[ru'' + (1+\nu)u' + 0.5(w')^2]w' + [ru' + \nu u + 1.5r(w')^2]w'' = -(1-\nu^2)rp_n. \tag{22}$$

In the application of the FvK theory, p_t is taken to be zero for both a normal pressure and a distributed vertical load, and p_n is taken to be the pressure and the vertical load, respectively (i.e, the right sides of Eqs. (21) and (22) are the same for normal or vertical loading).

The stress resultants are

$$n_r = [u' + 0.5(w')^2 + (\nu u/r)]/(1-\nu^2), \quad n_\theta = [(u/r) + \nu u' + 0.5\nu(w')^2]/(1-\nu^2). \tag{23}$$

3 Radial stretching

In some investigations, the inner or outer edge of a flat annular membrane is pulled radially (or both edges are pulled), causing tension and sometimes inducing wrinkles in the neighborhood of the inner edge (e.g., [16–22]). Applications of this problem occur in forming of metal sheets [23], cell and tissue biomechanics [24,25], and healing of skin wounds [26].

Two cases are considered here. One will be called "pulling inward:" the outer edge is fixed and the inner edge is pulled inward by a radial displacement U_1. The other case will be called "pulling outward:" the inner edge is fixed and the outer edge is pulled outward by a radial displacement U_2. The nondimensional boundary conditions are $u(a) = -u_1$ and $u(1) = 0$ for pulling inward, and $u(a) = 0$ and $u(1) = u_2$ for pulling outward, where $u_j = U_j/B$ for $j = 1, 2$, and $u_j > 0$.

For the FvK, R, and GR theories, with $w = \phi = p_t = p_n = 0$, the equilibrium equations reduce to the linear equation

$$r^2u'' + ru' - u = 0. \tag{24}$$

For pulling outward, the solution of Eq. (24) is [17]

$$u(r) = u_2(r^2 - a^2)/[r(1-a^2)]. \tag{25}$$

The circumferential stress resultant n_θ is always positive, and wrinkling does not occur. For the R and FvK theories, the stress resultants can be written as

$$\begin{aligned} n_r(r) &= u_2[(1+\nu)r^2 + (1-\nu)a^2]/[(1-\nu^2)(1-a^2)r^2], \\ n_\theta(r) &= u_2[(1+\nu)r^2 - (1-\nu)a^2]/[(1-\nu^2)(1-a^2)r^2]. \end{aligned} \tag{26}$$

For pulling inward, the solution of Eq. (24) is [17]

$$u(r) = -u_1a(1-r^2)/[r(1-a^2)]. \tag{27}$$

Material is pulled into regions with smaller circumferential lengths, and n_θ may become negative, which leads to wrinkling [8]. The stress resultants for the R and FvK theories take the form

$$\begin{aligned} n_r(r) &= u_1a[(1+\nu)r^2 + (1-\nu)]/[(1-\nu^2)(1-a^2)r^2], \\ n_\theta(r) &= u_1a[(1+\nu)r^2 - (1-\nu)]/[(1-\nu^2)(1-a^2)r^2]. \end{aligned} \tag{28}$$

Hence, for wrinkling not to occur, $r > r^*$ is needed where (for the GR, R, and FvK theories)

$$r^* = [(1-\nu)/(1+\nu)]^{1/2} \tag{29}$$

[17–20]. This condition is independent of the magnitude of u_1.

Values of r^* for $\nu = 0.1, 0.2, 0.3, 0.4$ and 0.5, respectively, are 0.905, 0.816, 0.734, 0.655 and 0.577. The displacement in Eq. (27) is only valid if $a > r^*$, which restricts the annular membrane to be narrow, especially

when ν is small, if wrinkling is to be avoided. The radial stress resultant n_r for pulling inward is positive when $a > r^*$, and decreases as r increases from $r = a$ (with $a \geq r^*$) to $r = 1$.

Radial displacements $u(r)$ normalized by the specified edge displacement are plotted in Fig. 2. The two curves in the bottom half of the figure are from Eq. (27) for pulling inward where $u(r) < 0$ between the edges, with $j = 1$, $a = 0.6$ and 0.8, $u(a)/u_1 = -1$, and $u(1)/u_1 = 0$. The curves are independent of ν, but are only valid if $a > r^*$. Using $a = r^* = 0.6$ in Eq. (29), one finds that the left curve is only valid if $\nu > 0.47$, and similarly, the right curve is only valid if $\nu > 0.22$. The curves in the top half of Fig. 2 for pulling outward ($j = 2$) are obtained from Eq. (25) with $a = 0.2$, 0.4, 0.6, and 0.8, $u(a)/u_2 = 0$, and $u(1)/u_2 = 1$.

4 Vertical displacement at inner edge

As mentioned in Sect. 2.2, the displacements and strains obtained with the R and GR theories are the same for problems considered in this section. In the nondimensional equilibrium equations, $p_t = p_n = 0$.

4.1 Annular membrane

In this subsection, the outer edge is fixed and the inner edge is displaced downward by a distance $W_1 > 0$. This problem is related to punching (indentation) of a membrane by a cylindrical body (e.g., [27]) and to a pull-off test for adhesion described in Sect. 4.2. Studies considering such a transverse edge displacement include [28–35].

*No radial stretching.*The boundary conditions are $w(a) = w_1$ and $u(a) = u(1) = w(1) = 0$. The stress resultants n_r and n_θ are positive, and they decrease as r increases from $r = a$ to $r = 1$. For $\nu = 1/3$, the FvK theory has a closed-form solution in which there is no radial displacement (e.g., [31,36]):

$$w(r) = w_1(1 - r^{2/3})/(1 - a^{2/3}), \quad u(r) = 0, \quad n_r(r) = 3n_\theta(r) = w_1^2/[4(1 - a^{2/3})^2 r^{2/3}]. \tag{30}$$

For all other values of ν, $u(r)$ is very small compared to $w(r)$. The sign of $u(r)$ for $a < r < 1$ is positive if $\nu < 1/3$ and negative if $\nu > 1/3$. The function $w(r)$ in Eq. (30) is almost linear. The stress resultant $n_r(r)$, normalized by w_1^2, is plotted in Fig. 3 for $a = 0.2$, 0.4, 0.6, and 0.8. As seen in Eq. (30), $n_\theta(r)$ has the same shape as $n_r(r)$ but with a magnitude one-third as large.

Some cases were examined numerically with the GR theory. In the shooting method, the values of $u'(a)$ and $\phi(a)$ are varied until the boundary conditions at $r = 1$ are satisfied with sufficient accuracy. In most cases for parameters w_1, a, and ν for which the maximum strain $\varepsilon_r(a)$ is less than 0.05, the maximum magnitudes of $u(r)$ computed using the GR theory are slightly smaller than those from the FvK theory. The case $\nu = 1/3$ is an exception, in which $u(r)$ from the GR theory is very small, whereas $u(r)$ from the FvK theory is zero.

Inward radial stretching. Now the annular membrane is assumed to be displaced downward at the inner edge with $w(a) = w_1$, and then stretched radially inward at the inner edge, so that $u(a) = -u_1$. For the R and GR theories, $u'(a)$ and $\phi(a)$ are varied until $u(1) = w(1) = 0$; for the FvK theory, $u'(a)$ and $w'(a)$ are varied.

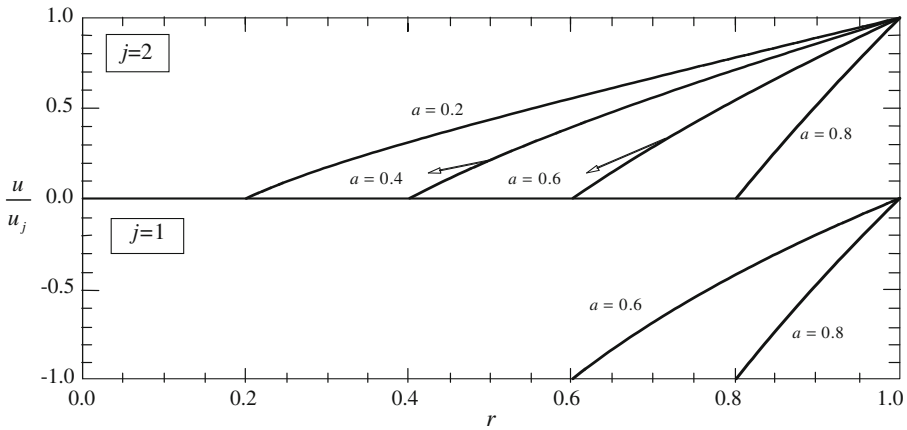

Fig. 2 Normalized radial displacement $u(r)/u_j$ for pulling inward ($j = 1$) and pulling outward ($j = 2$)

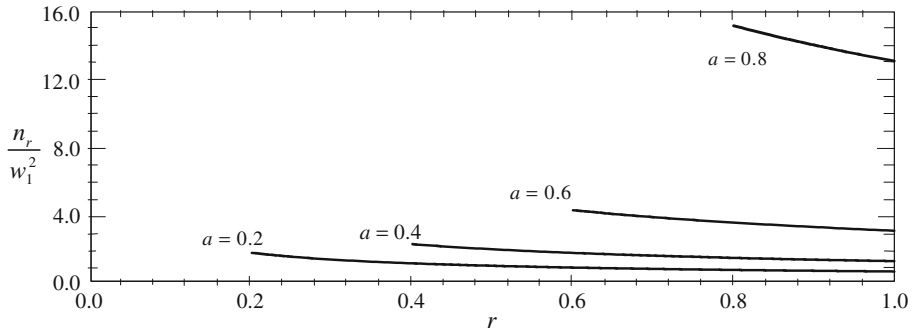

Fig. 3 Vertical displacement w_1 at inner edge: normalized meridional stress resultant $n_r(r)/w_1^2$ versus r; $\nu = 1/3$; FvK theory

The effect of w_1 on the wrinkling theshold radius r^* is investigated. The condition $n_\theta(a) = 0$ is used as a boundary condition. For the FvK theory, $u'(a) = [u_1/(\nu a)] - 0.5[w'(a)]^2$ is used, and a and $w'(a)$ are varied. The resulting solution for a gives r^*. For the R and GR theories, $u'(a) = [(u_1 \cos\phi(a)/(\nu a)] - 1 + \cos\phi(a)$.

When $w_1 = 0$, the value of r^* is given in Eq. (29) and is independent of u_1. For $w_1 \neq 0$, r^* depends on u_1 and w_1 as well as ν. Some results showing the dependence of r^* are presented in Figs. 4 and 5 using the FvK theory. In Fig. 4, $u_1 = 0.003$ and r^* is plotted as a function of w_1 for $\nu = 0.1, 0.3$, and 0.5. It is seen that r^* decreases as w_1 or ν increases. In the figure, the maximum strain is 0.05 at the right end of the upper curve, and lower elsewhere. In Fig. 5, $w_1 = 0.01$. The maximum strain is greater than 0.05 for $\nu = 0.1$ and $u_1 > 0.0045$, and less otherwise. The threshold radius r^* increases as u_1 increases.

Computations with the R and GR theories were made to compare values of r^* to those in Figs. 4 and 5. It was found that the values are slightly higher for the R and GR theories, but the differences are insignificant.

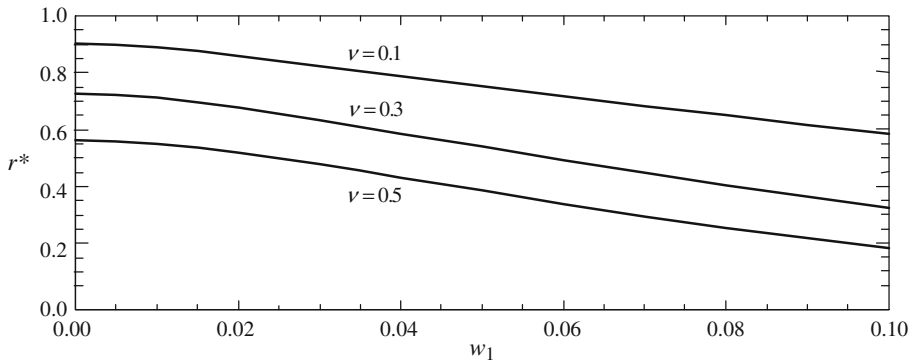

Fig. 4 Vertical displacement w_1 at inner edge: minimum inner-edge radius r^* for no wrinkling versus w_1; $u_1 = 0.003$; $\nu = 0.1, 0.3, 0.5$; FvK theory

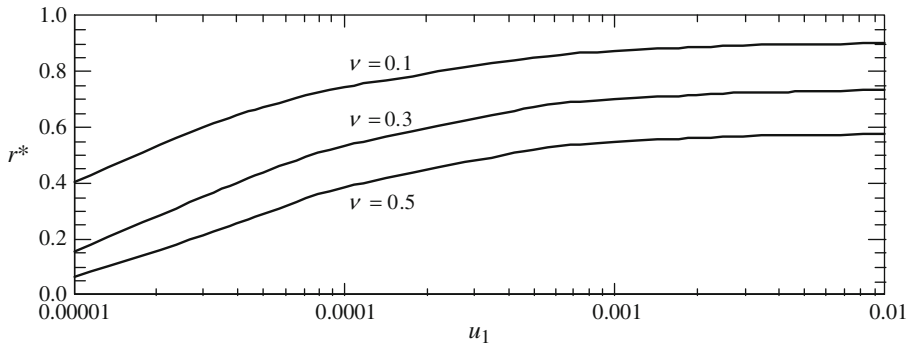

Fig. 5 Vertical displacement w_1 at inner edge: r^* versus u_1; $w_1 = 0.01$; $\nu = 0.1, 0.3, 0.5$; FvK theory

4.2 Adhesive punch pull-off test on circular blister

This type of analysis is relevant to an adhesive pull-off test in which a rigid, vertical, circular cylindrical punch is in adhesive contact axisymmetrically with a horizontal, circular (not annular) membrane whose edge is fixed. The cylinder is pulled upward and the membrane slowly debonds from the cylinder, with decreasing contact radius, until the membrane suddenly separates from the punch at a finite contact radius. Fig. 6 depicts the cross section along a diameter, in nondimensional terms.

This problem has been analyzed in [37–42]. The analysis in the last five of these papers considered a cylindrical radius just smaller than the membrane radius, and applied approximate solutions, mostly assuming (i) that n_r and n_θ are equal and independent of r, or sometimes assuming (ii) that $w(r)$ is linear.

As an example, the closed-form solution in Eqs. (30) is considered, with the FvK theory and $\nu = 1/3$. In nondimensional terms, the circular membrane is fixed at $r = 1$, and a flat punch is adhered to the membrane for $0 \le r \le a$. The punch is displaced upward with deflection $w_1 (< 0)$ and total force f (Fig. 6). The adhesion energy (or critical strain energy release rate) is denoted $(\Delta\gamma)_N$. The quantities f and $(\Delta\gamma)_N$ are related to the dimensional upward force F and adhesion energy $(\Delta\gamma)_D$ by

$$f = F/(EhB), \quad (\Delta\gamma)_N = (\Delta\gamma)_D/(Eh). \tag{31}$$

Vertical equilibrium of the bottom of the punch gives, with the use of Eqs. (30),

$$f = 2\pi a n_r(a) w'(a) = -(\pi/3) w_1^3 (1 - a^{2/3})^{-3}. \tag{32}$$

Following [39], the nondimensional net input energy is

$$U_T = f|w_1| - \pi a^2 (\Delta\gamma)_N - (\pi/12) w_1^4 (1 - a^{2/3})^{-3}, \tag{33}$$

where the first term represents the work done by the punch, the second term represents the surface energy of adhesion, and the last term is the negative of the membrane strain energy [43] computed with w and u given in Eqs. (30). For debonding to occur, the derivative of U_T with respect to the bonded area πa^2 is set equal to zero. After substituting Eq. (32) into Eq. (33), this calculation furnishes a formula for w_1 in terms of a and $(\Delta\gamma)_N$, which can be used to give f in terms of a and $(\Delta\gamma)_N$, and then a can be eliminated between those two formulas to give w_1 in terms of f and $(\Delta\gamma)_N$. The three formulas are

$$w_1 = -2^{1/2} (\Delta\gamma)_N^{1/4} (a^{1/3} - a), \quad f = (2/3) 2^{1/2} \pi a (\Delta\gamma)_N^{3/4},$$

$$w_1 = [3/(2\pi)] (\Delta\gamma)_N^{-1/2} f - (3f/\pi)^{1/3}. \tag{34}$$

Based on the last of these equations, as the cylinder is pulled upward and w_1 decreases, w_1 reaches a limit when $\mathrm{d}w_1/\mathrm{d}f = 0$, which leads to

$$a = 27^{-1/2} = 0.1925, \quad w_1 = -0.5443 (\Delta\gamma)_N^{1/4}, \quad f = 0.5700 (\Delta\gamma)_N^{3/4}. \tag{35}$$

In other words, for $\nu = 1/3$ and FvK theory, the membrane suddenly separates from the cylinder when the contact radius decreases to 0.1925 times the radius of the outer edge, independently of the adhesion energy $(\Delta\gamma)_N$. Very similar values $a = 0.1945$ and 0.1932 were found in [38] using assumptions (i) and (ii), respectively, for any values of $(\Delta\gamma)_N$ and ν, even though the approximate functions used there for $w(r)$, $n_r(r)$, and $n_\theta(r)$ are quite different from those in Eqs. (30) that satisfy the FvK equations for $\nu = 1/3$.

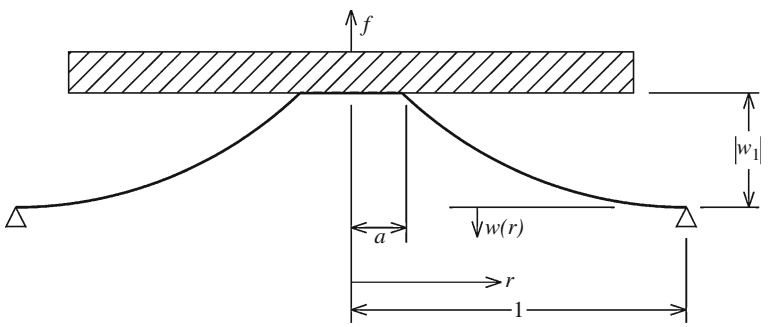

Fig. 6 Cross section along diameter of circular membrane in adhesive punch pull-off test

5 Transverse pressure

In this section, a dimensional uniform transverse pressure P_0 acts on the membrane. In nondimensional terms, $p_t = 0$ and $p_n = p_0 = P_0 B/(Eh)$. In the FvK theory, $w(r)$ is proportional to $p_0^{1/3}$, and $u(r)$, strains, and stress resultants are proportional to $p_0^{2/3}$. Wrinkling does not occur. Annular and circular membranes are considered.

5.1 Annular membrane

The geometry along a diameter is shown in Fig. 7 in nondimensional terms. The island blister test for adhesion [14,44–46] is an application of this problem, with debonding occurring at the inner radius $r = a$. Here the annular membrane is fixed at $r = a$ and $r = 1$, with $u = w = 0$ at those radii. In the shooting method, the values of $u'(a)$ and either $\phi(a)$ or $w'(a)$ are varied until the boundary conditions at $r = 1$ are satisfied with sufficient accuracy. Wrinkling does not occur.

The maximum transverse deflection $w_{\max}$ is larger when computed using the GR and R theories than from the FvK theory. For example, if $\nu = 0.3, a = 0.3$ and $p_0 = 0.04$, which yields a maximum strain $\varepsilon_r(a)$ approximately equal to 0.05, the values of $w_{\max}$ for the GR, R, and FvK theories, respectively, are 0.0770, 0.0763 and 0.0755. For the GR and R theories, the proportionality relationships described above are approximately satisfied. In Fig. 8, $w_{\max}$ is plotted as a function of a using the GR theory for the case $p_0 = 0.01$, with the lower and upper curves representing the cases $\nu = 0.5$ and $\nu = 0$, respectively. The maximum strain is less than 0.05 except near the left end of the curve for $\nu = 0$.

5.2 Circular membrane with rigid horizontal constraint (constrained blister test)

A circular (not annular) membrane is considered in this subsection, as shown in Fig. 9 in nondimensional terms along a diameter. The origin is at the center of the membrane. The membrane is subjected to pressure from above. The transverse deflection is restricted by a rigid, horizontal, frictionless surface at a vertical distance

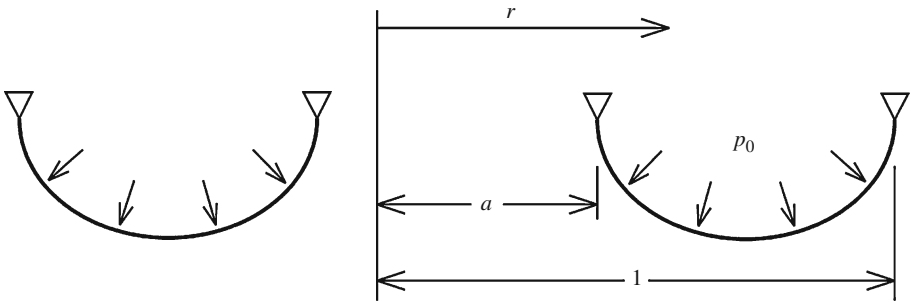

Fig. 7 Cross section along diameter of annular membrane under transverse pressure

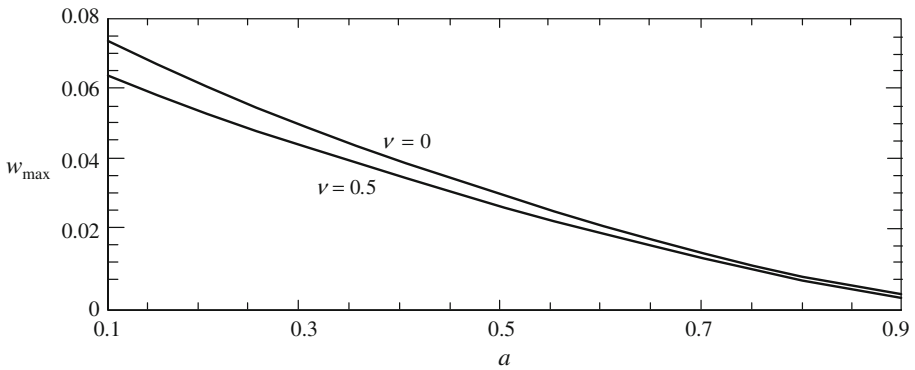

Fig. 8 Transverse pressure: maximum transverse displacement $w_{\max}$ versus inner radius a; $p_0 = 0.01$; $\nu = 0, 0.5$; GR theory

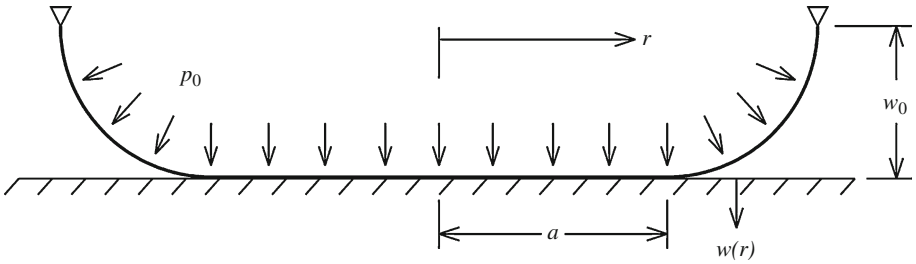

Fig. 9 Cross section along diameter of circular membrane with rigid constraint

w_0 below the edge ($r = 1$), and the contact radius $r = a$ is unknown a priori. This configuration is found in the constrained blister test for adhesion, with debonding occurring at $r = 1$ (e.g., [37,47,48]). For a fixed edge at $r = 1$, the effect of adhesion on the contact area πa^2 was analyzed in [43].

For $0 \le r \le a$, $w = 0$ and $u = Cr$ where C is a constant, so that $u = ru'$. The boundary conditions at $r = a$ are $u = au'$, $w = 0$, and either $w' = 0$ (FvK theory) or $\phi = 0$ (R and GR theories), and at $r = 1$ they are $u = 0$ and $w = -w_0$. In the shooting method, it is easier to specify a rather than w_0, and to obtain w_0 as the value of $-w(1)$ in the solution. The unknown quantity $u'(a)$ is varied until the boundary condition $u(1) = 0$ is satisfied.

Some shapes $w(r)$ using the FvK theory are presented in [43] along with the effect of the pressure on the contact radius. Computations using Eqs. (9) and (10) show that for given values of ν, w_0 and p_0, and for a sufficiently small range of the contact radius a, the value of a obtained with the GR theory is larger than that from the FvK theory. However, if a is sufficiently large, the opposite is true. For example, assume that $\nu = 0.3$ and $w_0 = 0.11$. For $p_0 = 0.005$, the FvK, R, and GR theories yield, respectively, $a = 0.0582$, 0.0607 and 0.0718. For $p_0 = 0.02$, they give $a = 0.474$, 0.473 and 0.479. Finally, for $p_0 = 0.2$, they provide $a = 0.763$, 0.755 and 0.760.

5.3 Circular membrane

By letting $a \to 0$ in the numerical analysis of the previous subsection, one can obtain results for a circular membrane fixed at its edge ($r = 1$) and subjected to a normal pressure (with no rigid constraint). The classical analysis in [49] is often cited with regard to this problem.

Numerical results based on the FvK theory (using $a = 10^{-9}$) are presented in Table 1 for $\nu = 0$, 0.1, 0.2, 0.3, 0.4, and 0.5. Values of the depth w_0, radial strain at the center ($r = 0$), radial strain at the edge ($r = 1$), radial stress resultant at $r = 0$ (which is the same as the circumferential stress resultant there), radial stress resultant at $r = 1$, and circumferential stress resultant at $r = 1$ are listed. For $\nu = 0.3$, the value of w_0 was given in [43], and similar values have been computed by others in earlier studies. The values of w_0 and $n_r(0)$ are similar to those in [50] except for w_0 for $\nu = 0.1$. The maximum strain occurs at $r = 0$ if $\nu = 0$, 0.1 and 0.2, and at $r = 1$ if $\nu = 0.3$, 0.4 and 0.5. The radial displacement $u(r)$ has its maximum value near $r = 0.61$.

Peddieson [51] applied the R theory in terms of a stress function instead of $u(r)$, for the same values of ν and for five values of p_0 (up to $p_0 = 0.16$). Using the present equations and shooting procedure, the results for w_0 are within a few percent of his, sometimes lower and sometimes higher. They are slightly higher than the

Table 1 Effect of Poisson's ratio ν or circular membrane with transverse pressure; FvK theory

ν	0	0.1	0.2	0.3	0.4	0.5
$w_0/(p_0^{1/3})$	0.71832	0.69890	0.67744	0.65344	0.62626	0.59488
$\varepsilon_r(0)/(p_0^{2/3})$	0.4051	0.3710	0.3365	0.3018	0.2665	0.2307
$\varepsilon_r(1)/(p_0^{2/3})$	0.2894	0.2988	0.3035	0.3030	0.2967	0.2838
$n_r(0)/(p_0^{2/3})$	0.4051	0.4122	0.4207	0.4311	0.4442	0.4613
$n_r(1)/(p_0^{2/3})$	0.2894	0.3018	0.3161	0.3330	0.3532	0.3784
$n_\theta(1)/(p_0^{2/3})$	0	0.0302	0.0632	0.0999	0.1413	0.1892

values of w_0 from the FvK theory, and the GR theory produces even higher values. For $\nu = 0.3$, the maximum strain is 0.05 when $p_0 = 0.065$ and the corresponding central transverse displacement is about one-eighth of the diameter of the membrane. For this case, $w_0 = 0.2627, 0.2649$ and 0.2739, respectively, from the FvK, R and GR theories. At $p_0 = 0.01$, the corresponding values are $w_0 = 0.1408, 0.1411$ and 0.1424. (For the R and GR theories, $\phi(a) = 10^{-7}$ and $a = 10^{-9}$ are used to avoid numerical problems.)

Pai [52] listed the results for the example of $P_0 = 5.51581\,\text{GPa}$, $B = 1.5\,\text{m}$, $h = 0.0127\,\text{mm}$ and $\nu = 0.3$. He obtained a central deflection $W_0 = 18.6573\,\text{mm}$. From the present analysis, the results from the FvK, R, and GR theories, respectively, are $W_0 = 18.6556\,\text{mm}$, $18.6560\,\text{mm}$ and $18.6572\,\text{mm}$.

6 Ponding

In this section, the deformed membrane holds a liquid with dimensional specific weight γ_D and nondimensional specific weight $\gamma_N = \gamma_D B^2/(Eh)$. The liquid level is at the level of the outer edge of the membrane, i.e., full ponding is assumed. In the FvK theory, $w(r)$ is proportional to $\gamma_N^{1/2}$, and $u(r)$, strains, and stress resultants are proportional to γ_N. Wrinkling does not occur. Annular and circular membranes are considered.

6.1 Annular membrane

For the annular membrane, $u = w = 0$ at $r = a$ and $r = 1$ (similar to Fig. 7). In the equilibrium equations, $p_t = 0$ and $p_n = \gamma_N w$. Numerical results using the FvK theory with $\nu = 0.3$ are presented in Table 2. The largest transverse displacement $w_{\max}$ occurs near $r = (a + 1)/2$, i.e., near midway between the inner and outer edges, where the value of w will be denoted w_{mid}. For $a = 0.2, 0.4, 0.6$ and 0.8, w_{mid} and the maximum values of ε_r and n_r (which occur at the inner edge $r = a$) are listed. The values of w_{mid} are extremely close to the maximum values of $w(r)$.

The effect of ν on w_{mid} is shown in Table 3. For $a = 0.2, 0.4, 0.6$ and 0.8, values of $w_{\text{mid}}/(\gamma_{\text{N}}^{1/2})$ from the FvK theory are listed for $\nu = 0, 0.1, \ldots, 0.5$. As expected, the transverse displacement decreases as either ν or a increases.

The R and GR theories yield larger values of $w_{\max}$ then the FvK theory. When the maximum strain is 0.05 for the FvK results with $\nu = 0.3$, for $a = 0.2, 0.4, 0.6$ and 0.8, respectively, the maximum transverse displacements $w_{\max}$ given by the R theory are larger by 1.2, 1.6, 1.8 and 2.1%, and for the GR theory they are larger by 2.6, 3.5, 4.1 and 4.7%.

6.2 Circular membrane

Results for full ponding of a circular membrane, fixed at its edge, were presented in [53,54]. The numerical procedure used in this subsection is similar to that described in Sect. 5.3. Here the origin is on the membrane at $r = 0$ (actually at $r = a = 10^{-9}$ in the computations), and the depth at $r = 0$ is denoted w_0 (similar to

Table 2 Effect of inner radius a on annular membrane with ponding; FvK theory, $\nu = 0.3$

a	0.2	0.4	0.6	0.8
$w_{\text{mid}}/[(\Delta\gamma)_N^{1/2}]$	0.129	0.0707	0.0311	0.00774
$\varepsilon_r(a)/(\Delta\gamma)_N$	0.126	0.0494	0.0181	0.00401
$n_r(a)/(\Delta\gamma)_N$	0.139	0.0542	0.0199	0.00441

Table 3 Effect of Poisson's ratio ν on $w_{\text{mid}}/(\gamma_N^{1/2})$ for annular membrane with ponding; FvK theory

ν	0	0.1	0.2	0.3	0.4	0.5
$a = 0.2$	0.140	0.137	0.134	0.129	0.123	0.116
$a = 0.4$	0.0751	0.0743	0.0729	0.0707	0.0678	0.0640
$a = 0.6$	0.0327	0.0325	0.0320	0.0311	0.0298	0.0282
$a = 0.8$	0.00812	0.00808	0.00795	0.00774	0.00744	0.00703

Fig. 9 with $a = 0$). In the equilibrium equations, $p_t = 0$ and $p_n = \gamma_N(w_0 + w)$. The boundary conditions are $u = w = 0$ and either $w' = 0$ or $\phi = 0$ at $r = 0$, and $u = 0$, $w = -w_0$ at $r = 1$. In the shooting procedure, the unknowns are $u'(0)$ and w_0. For the R and GR theories, $\phi(a) = 10^{-7}$ was used in the computer program to avoid numerical problems.

First, the example treated in [53,54] is analyzed, in which the dimensional radius is $B = 1.857\,\text{m}$, $\gamma_D = 9.8\,\text{kN/m}^3$ (water), $E = 208\,\text{GPa}$ (304 stainless steel), $h = 0.051\,\text{mm}$, and $\nu = 1/3$. The FvK theory here gives $W(0) = 5.07\,\text{cm}$, $U_{\max} = 0.287\,\text{mm}$, and stresses $\sigma_r(0) = \sigma_\theta(0) = 144.13\,\text{MPa}$, $\sigma_r(B) = 100.78\,\text{MPa}$, and $\sigma_\theta(B) = 33.59\,\text{MPa}$. These values are slightly higher than those in the two references.

Consider the case $\nu = 1/3$ and $\gamma_N = 0.35$, which has a maximum strain of $\varepsilon_r(0) = 0.05$ in the FvK theory. Results for w_0 (the magnitude of the central deflection), $\varepsilon_r(0)$, $n_r(0)$, $n_r(1)$, $n_\theta(1)$, and $u_{\max}$ from the FvK, R, and GR theories are listed in Table 4. The stress resultants at $r = 1$ are slightly lower for the R theory than for the FvK theory. All the values for the GR theory are higher than those for the FvK and R theories.

In order to compare the results of the three theories up to large strains, the nondimensional depth w_0 is plotted as a function of the nondimensional specific weight γ_N in Fig. 10 for $\nu = 1/3$. The lower (solid) curve corresponds to the FvK results, the intermediate (dashed) curve to the R theory, and the top (dotted) curve to the GR theory. The FvK curve is given by $w_0 = 0.4742(\gamma_N)^{1/2}$. The maximum strain is 0.05 when $\gamma_N = 0.35$, 0.34, and 0.31, respectively, in the FvK, R, and GR results. At the right end of the figure ($\gamma_N = 1$), the maximum strain is 0.14, 0.16, and 0.24, respectively, in the FvK, R, and GR results.

7 Vertical distributed loading, with vertically sliding outer edge

The motivation for the problem analyzed in this section comes from geotechnical engineering [55,56]. Circular piles are sometimes used to strengthen soft soils underneath embankments. One or more layers of a geosynthetic material may be placed horizontally over the piles to distribute the downward loading toward the piles and away from the soft soil. The deflections, strains, and tensions in these membranes need to be predicted. An axisymmetric model involving one pile is often used for analytical purposes. Since this is a "unit cell" for one pile in a periodic array, the radial displacement and the slope of the membrane at the outer boundary are assumed to be zero. Also, the membrane directly over the pile is almost flat and then drops sharply into the soil lying outside the pile, so that the membrane is sometimes assumed to be pinned at the edge of the pile, and thus to have an annular shape. The geometry along a diameter is depicted in nondimensional terms in Fig. 11.

Table 4 Results from three theories for circular membrane with ponding; $\nu = 1/3$, $\gamma_N = 0.35$

	FvK theory	R theory	GR theory
w_0	0.2805	0.2849	0.3000
$\varepsilon_r(0)$	0.0498	0.0517	0.0572
$n_r(0)$	0.0747	0.0775	0.0811
$n_r(1)$	0.0522	0.0520	0.0570
$n_\theta(1)$	0.0174	0.0173	0.0181
$u_{\max}$	0.0165	0.0172	0.0188

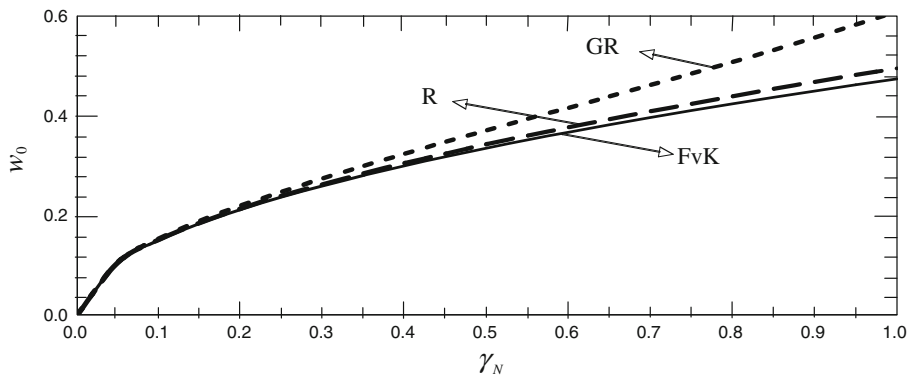

Fig. 10 Ponding on circular membrane: central transverse displacement versus specific weight of liquid; $\nu = 1/3$; FvK, R, and GR theories

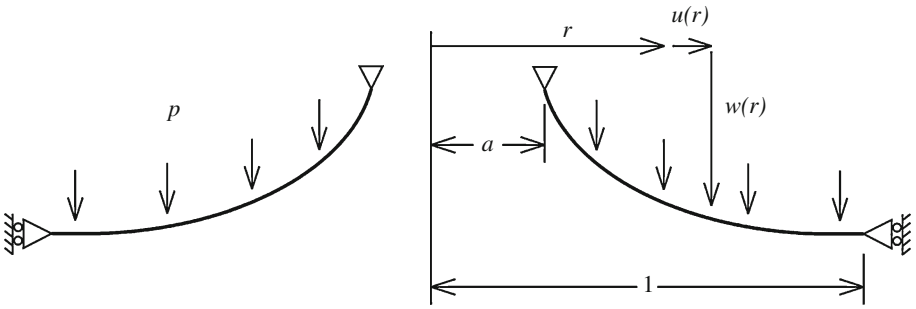

Fig. 11 Cross section along diameter of annular membrane with sliding outer edge; vertical loading

The vertical loading is assumed to have the constant dimensional value P per unit of undeformed area of the horizontal projection of the membrane. For the GR theory,

$$P_t = P \sin\phi/[(1+\varepsilon_r)(1+\varepsilon_\theta)], \quad P_n = P\cos\phi/[(1+\varepsilon_r)(1+\varepsilon_\theta)]. \tag{36}$$

For the R theory, the denominators in Eqs. (36) become unity. The right sides of Eqs. (9) and (14) become $-(1-\nu^2)r^2(\sin\phi\cos^2\phi)p$, and the right sides of Eqs. (10) and (15) become $-(1-\nu^2)r^2(\cos^2\phi)p$, where $p = PB/(Eh)$. Therefore the displacements based on the R and GR theories are the same, as mentioned in Sect. 2.2. For the FvK theory, $P_t = 0$ and $P_n = P$, and in Eqs. (21) and (22), respectively, $p_t = 0$ and $p_n = p$.

The boundary conditions are $u(a) = w(a) = 0$, $u(1) = 0$, and either $w'(1) = 0$ (FvK theory) or $\phi(1) = 0$ (R and GR theories). To obtain numerical solutions of the equilibrium equations, the quantities $u'(a)$ and either $w'(a)$ or $\phi(a)$ are varied until the boundary conditions at $r = 1$ are satisfied. In the FvK theory, $w(r)$ is proportional to $p^{1/3}$, and $u(r)$, strains, and stress resultants are proportional to $p^{2/3}$. Attention is focused on the vertical displacement $w(1)$ at the outer edge, which is denoted w_2, and on conditions for the onset of wrinkling.

Table 5 presents values of $w_2/p^{1/3}$ for $a = 0.2, 0.4, 0.6$ and 0.8, with $\nu = 0.1, 0.2, \ldots, 0.5$. Where numbers are not listed, the minimum circumferential stress resultant n_θ is negative and wrinkling occurs. This case is different from previous ones in that wrinkling does not initiate at the inner edge $r = a$. The radial displacement $u(r)$ is zero at the inner and outer edges, and is negative internally. Hence points on the membrane move inward. The radius associated with the largest inward movement (i.e., minimum value of u) is near the radius with the minimum value of n_θ (where wrinkling begins).

Consider decreasing values of ν. For $a = 0.2$, n_θ decreases to zero at $r = 0.62$ when $\nu = 0.244$. For $a = 0.4$, n_θ decreases to zero at $r = 0.68$ when $\nu = 0.211$. For $a = 0.6$, n_θ decreases to zero at $r = 0.78$ when $\nu = 0.150$. For a $= 0.8$, n_θ decreases to zero at $r = 0.89$ when $\nu = 0.0769$.

Now assume that ν is fixed and a is reduced. For $\nu = 0.1$, n_θ decreases to zero at $r = 0.85$ when $a = 0.739$. For $\nu = 0.2$, n_θ decreases to zero at $r = 0.62$ when $a = 0.245$. For $\nu = 0.3$, 0.4, and 0.5, n_θ is positive for all values of a.

The displacements $w(1)$ based on the GR theory (and hence the same for the R theory) were computed for the cases in Table 5 with p chosen for each case such that the maximum strain $\varepsilon_r(a)$ is 0.05. The resulting displacements at the outer edge are between 1.3 and 1.8% higher than those in Table 5 from the FvK theory.

8 MEMS device

The MEMS device considered here exhibits an instability that can be utilized (as in a switch) or needs to be prevented. In dimensional terms, a horizontal rigid plate is situated below an initially flat membrane, with

Table 5 Effect of Poisson's ratio ν on $w_2/p^{1/3}$ for annular membrane with vertical load; FvK theory

ν	0.1	0.2	0.3	0.4	0.5
$a = 0.2$	–	–	0.771	0.755	0.734
$a = 0.4$	–	0.498	0.492	0.481	0.466
$a = 0.6$	–	0.278	0.274	0.268	0.259
$a = 0.8$	0.108	0.107	0.106	0.103	0.0993

an initial gap g_0. A voltage difference V_0 is applied, and the membrane deflects toward the plate due to the electrostatic Coulomb force. When the voltage reaches a critical value, the equilibrium state of the membrane becomes unstable and the membrane jumps downward and contacts the plate. This is called a pull-in instability.

Circular membranes exhibiting this instability were considered in [57–62] and elsewhere, with [60,61] including an analysis of annular membranes. An application of the annular geometry may occur in a micropump [63], and an annular plate (i.e., including bending stiffness) was analyzed in [64].

In [57]–[62], stretching of the membrane was neglected and a constant applied radial tension T was assumed to act on the membrane, initially and during deformation. The governing equation for the "standard model" is

$$T[W'' + (W'/r)] = P_{V_0} \quad \text{where} \quad P_{V_0} = \varepsilon_0 V_0^2/[(g_0 - W)^2]. \tag{37}$$

The quantity ε_0 is the permittivity of free space. In this model, the electrostatic pressure is inversely proportional to the square of the gap. Based on the form of Eq. (37), the pull-in voltage V_0^* is proportional to the 3/2 power of g_0.

Duan and Wan [65] analyzed a plate model. They also included stretching of the thin structure in a restricted way, using an average radial strain and assumption (i) described in Sect. 4.2, in which the radial and circumferential stress resultants are assumed to be equal and to be independent of the radius. There was no pre-tension, and the radial stress was proportional to an integral of $R(W')^2$ where R is the radial coordinate. Also, the authors replaced the electrostatic pressure in Eq. (37) by a constant (average) value in their approximate solution procedure. Based on their equations, the pull-in voltage V_0* is proportional to the 3/2 power of g_0 when bending dominates, and to the 5/2 power of g_0 when stretching dominates.

In this section, the formulations in Sect. 2 are utilized, which neglect bending stiffness. The radial displacement u is an unknown function of r, along with the stress resultants and transverse displacement. No pre-tension is required, although it can be included as in Sect. 3. The membrane is fixed (i.e., no transverse or radial displacements) at its outer edge $r = 1$, and also at its inner edge $r = a$ for the annular case. Unlike the analyses in [57]–[62] that are based on the structural model in Eq. (37), here the results depend on Poisson's ratio. For the FvK theory, the pull-in voltage V_0^* is proportional to the 5/2 power of g_0.

The standard electrostatic pressure P_{V_0} in Eq. (37) is used. It is assumed that this pressure is a downward force per unit of horizontal area. The nondimensional equilibrium equations are similar to those in Sect. 7 with p replaced by $p_{V_0}/[(\delta_0 - w)^2]$ where $p_{V_0} = \varepsilon_0 V_0^2/(2EhB)$ and $\delta_0 = g_0/B$ (the aspect ratio [59]). The nondimensional pull-in pressure magnitude will be denoted $p_{V_0}^*$.

8.1 Annular membrane

The numerical method for the annular membrane is similar to that described in Sect. 7. The curve of the forcing magnitude p_{V_0} versus a measure of the deflection (e.g., the maximum deflection) exhibits a turning (limit) point when pull-in instability occurs. Results were obtained for the case of an inner radius $a = 0.5$, Poisson's ratio $\nu = 0.1$, and nondimensional initial gap $\delta_0 = 0.05$.

Using the FvK theory, $p_{V_0}^* = 4.91 \times 10^{-6}$, with a corresponding maximum downward deflection $w_{\max} = 0.0328$ occurring at $r = 0.75$. The maximum slope magnitude is 0.20 (at $r = 1$), and the maximum radial strain is $\varepsilon_r(a) = 0.014$. If δ_0 were replaced by $c\delta_0$ while a and ν remained fixed, then $p_{V_0}^*$, w, and u would become $c^5 p_{V_0}^*$, cw, and $c^2 u$, respectively, so that $p_{V_0}^*$ is proportional to δ_0^5, and the dimensional pull-in voltage V_0* is proportional to $g_0^{5/2}$. Strains and stress resultants would be multiplied by c^2.

Using the R or GR theory, $p_{V_0}^* = 4.83 \times 10^{-6}$ and the corresponding maximum downward deflection $w_{\max} = 0.0322$ occurs at $r = 0.76$.

Wrinkling can occur before pull-in instability if ν is sufficiently small. For example, using the FvK, R, or GR theories, again with $a = 0.5$ and $\delta_0 = 0.05$, if p_{V_0} is very small (e.g., 1×10^{-10}) and if ν is decreased to 0.061, then n_θ decreases to zero at $r = 0.59$. The membrane would exhibit radial wrinkles in an annular region around $r = 0.59$ if $\nu < 0.061$.

8.2 Circular membrane

The numerical procedure is similar to the one used in Sect. 6.2 (with $a = 10^{-6}$ here). For this circular case, w is replaced by $w_0 + w$ in the pressure, where $w_0 = w(0)$ is the central transverse displacement of the

membrane. For $\nu = 0.1$ and $\delta_0 = 0.05$, all three theories give $p^*_{V_0} = 5.1 \times 10^{-8}$ with a corresponding central deflection $w^*_0 = 0.036$ (i.e., $0.72\delta_0$) at the onset of pull-in instability. The remaining results in this subsection are based on the FvK theory. Wrinkling does not occur for the cases considered.

Radial stretching is included here by changing the boundary condition $u(1) = 0$ to $u(1) = u_2$ (as used in Sect. 3). Table 6 presents results at the pull-off condition for the case $\nu = 0$. Results for radial stretching up to $u_2 = 5\delta_0^2$ are listed. Based on these values, for a given initial gap, the pull-in pressure magnitude $p^*_{V_0}$ is almost a linear function of u_2 except near $u_2 = 0$ (as are the strains and stress resultants). The central displacement at pull-in, w^*_0, decreases and then essentially becomes constant with $w^*_0 = 0.46\delta_0$ when u_2 becomes sufficiently large. The radial stress resultant n_r is not independent of the radius, but is larger at the center ($r = 0$) than at the edge ($r = 1$) of the membrane. However, the ratio between the central and edge values of n_r approaches unity as the magnitude of outward stretching increases.

The results can be related to the parameter $\lambda = \varepsilon_0 V_0^2/(2Tg_0^3)$ used in [57–61], where the membrane tension T is assumed to be constant and stretching is neglected. Using that theory, the pull-in value λ^* was reported to be 0.789 [59,61] and the value of w^*_0/δ_0 to be 0.4365 [59]. Here the parameter corresponding to λ^* is $\xi^* = p^*_{V_0}/(n^*_r\delta_0^3)$, but the stress resultant n_r is not constant in the membrane. If the value $n^*_r(1)$ at the edge is used, the value of ξ^* is 0.79 or 0.80 for the cases in Table 6 except at $u_2 = 0$, where it is 0.76.

The pull-in pressure and deflection in [57–62] and [65] do not depend on Poisson's ratio ν. For the FvK theory, the ratio w^*_0/δ_0, listed in Table 6 for $\nu = 0$, is almost the same for any value of ν ($0 < \nu \le 0.5$). This is also true for ξ^*. However, $p_{V_0}{}^*$ essentially doubles as ν increases from 0 to 0.5, and $p_{V_0}{}^*$ is approximately proportional to $1/(1-\nu)$. Therefore, for any value of $u_2/(\delta_0^2)$ in Table 6, one can divide the value of $p^*_{V_0}/(\delta_0^5)$ in the table by $1-\nu$ to obtain an approximate value of $p^*_{V_0}/(\delta_0^5)$ for any value of ν ($0 < \nu \le 0.5$).

The FvK, R, and GR equations given in Sect. 2 could be used with more general formulations of the electrostatic force, such as the "corner-corrected" theory in [59], inclusion of the Casimir force [61], or a permittivity that varies with the radius [62].

9 Torsion at inner edge

A number of studies have considered torsion of the inner edge of a planar annular membrane (e.g., by a rigid hub) under initial tension. They include [66–87].

The problem involves the dimensional circumferential displacement $V(R)$, which is not included in the R and GR theories described in Sect. 2. Therefore only the FvK theory will be utilized. The strain ε_θ is given in Eq. (3b) and ε_r is given in Eq. (17). The dimensional shear stress resultant $N_{r\theta}(R)$ and shear strain $\varepsilon_{r\theta}(R)$ satisfy the following equilibrium equation (with $P_t = P_n = 0$), stress–strain relationship, and strain–displacement relationship [88]:

$$rN'_{r\theta} + 2N_{r\theta} = 0, \quad N_{r\theta} = Eh\varepsilon_{r\theta}/[2(1+\nu)], \quad \varepsilon_{r\theta} = V' - (V/R). \tag{38}$$

In terms of the nondimensional displacement $v_e = V/B$, these equations lead to the equilibrium equation

$$r^2 v''_e + r v'_e - v_e = 0, \tag{39}$$

which is the same as Eq. (24) for $u(r)$. (The subscript e, for equilibrium, is included to avoid confusion with Poisson's ratio ν.) The general solution has the form $v_e(r) = c_1 r + (c_2/r)$ where c_1 and c_2 are constants.

Table 6 Results at pull-in instability of circular membrane with electrostatic force; FvK theory, $\nu = 0$

$u_2/(\delta_0^2)$	0	0.1	0.2	0.3	0.4	0.5	1	2	3	4	5
$p^*_{V_0}/(\delta_0^5)$	0.15	0.21	0.28	0.35	0.42	0.50	0.88	1.67	2.46	3.24	4.04
w^*_0/δ_0	0.71	0.65	0.62	0.59	0.56	0.55	0.50	0.46	0.46	0.46	0.46
$n^*_r(0)/(\delta_0^2)$	0.36	0.40	0.48	0.55	0.63	0.72	1.18	2.15	3.15	4.14	5.14
$n^*_r(1)/(\delta_0^2)$	0.20	0.27	0.35	0.44	0.52	0.62	1.10	2.09	3.08	4.08	5.08

In nondimensional terms, the membrane is subjected to an outward displacement u_2 at its outer edge, and then to a circumferential displacement $v_1 > 0$ at its inner edge. The governing equations for $u(r)$ and $v_e(r)$ are linear and uncoupled. The solution for $u(r)$ is given by Eq. (25), and the solution for $v_e(r)$ is

$$v_e(r) = v_1 a(1 - r^2)/[r(1 - a^2)]. \tag{40}$$

The stress resultant $n_{r\theta}(r)$ is given by

$$n_{r\theta}(r) = -v_1 a/[(1 + \nu)(1 - a^2)r^2], \tag{41}$$

where $n_{r\theta} = N_{r\theta}/(Eh)$.

At the onset of wrinkling, the minimum principal stress $n_{\min}$ becomes zero, where

$$n_{\min} = 0.5(n_r + n_\theta) - [n_{r\theta}^2 + 0.25(n_r - n_\theta)^2]^{1/2}. \tag{42}$$

This occurs when $n_r n_\theta = n_{r\theta}^2$, which is satisfied first at the inner edge $r = a$ as v_1 is increased.

For outward radial stretching, with the use of Eqs. (26) and (41) for the stress resultants, one obtains the condition that the membrane remains taut as long as $v_1 < v_1^*$ where

$$v_1^* = 2au_2\nu^{1/2}/(1 - \nu). \tag{43}$$

If there is no radial stretching, the membrane wrinkles as soon as any circumferential displacement is applied. When $v_1 = v_1^*$, the orientations ψ of the minimum principal stress with respect to the tangent to the inner edge are obtained from $\tan(2\psi) = 2n_{r\theta}/(n_\theta - n_r) = v_1^*/(au_2) = 2\nu^{1/2}/(1 - \nu)$. For $\nu = 0$, 0.1, 0.2, 0.3, 0.4 and 0.5, respectively, they are 0, 17.5, 24.1, 28.7, 32.3 and 35.2 degrees, respectively. This implies that the angle of the wrinkles with respect to the circumference at the inner edge, which is related to the direction of the maximum principal stress, decreases as ν increases.

For inward radial stretching, with the use of Eqs. (28) and (41), one finds that the membrane remains taut as long as $v_1 < v_1^{**}$ where

$$v_1^{**} = u_1^{1/2}[(1 + \nu)^2 a^4 - (1 - \nu)^2]^{1/2}/(1 - \nu) \tag{44}$$

and a must be larger than r^* in Eq. (29), i.e., the right side of Eq. (44) must be real. When $v_1 = v_1^{**}$, the orientations ψ of the minimum principal stress with respect to the tangent to the inner edge are obtained from $\tan(2\psi) = v_1^{**}/u_1$, and in this case they depend on the inner radius a and the magnitude u_1 of the radial stretching as well as Poisson's ratio ν. At the onset of wrinkling, the resulting angle of the wrinkles with respect to the inner edge decreases as ν increases, decreases as a increases, and increases as u_1 increases.

If the inner edge is fixed and the outer edge is given a circumferential displacement $v_2 > 0$, Eq. (40) is replaced by

$$v_e(r) = v_2(r^2 - a^2)/[r(1 - a^2)] \tag{45}$$

and v_1 is replaced by $-v_2 a$ in Eq. (41). On the left sides of Eqs. (43) and (44), v_1 is replaced by $v_2 a$.

10 Torsion and vertical displacement at inner edge

In this section the outer edge of the annular membrane is stretched, and then the inner edge is displaced downward (as in Sect. 4) and twisted (as in Sect. 9). This problem has been considered in [29,33,34] without radial stretching. The FvK theory is applied here.

The circumferential displacement is again given by Eq. (40). The radial and transverse displacements are determined numerically from Eqs. (21) and (22) with $p_t = p_n = 0$ and with boundary conditions $u(a) = 0$, $w(a) = w_1$, $u(1) = u_2$, and $w(1) = 0$. For given values of w_1 and u_2, the value v_1^* of v_1 for which the minimum principal stress is zero (i.e., $n_r n_\theta = n_{r\theta}^2$) is computed. This yields

$$v_1^* = [\nu(\varepsilon_r^2 + \varepsilon_\theta^2) + (1 + \nu^2)\varepsilon_r\varepsilon_\theta]^{1/2}(1 - a^2)r^2/[(1 - \nu)a] \tag{46}$$

in terms of the strains ε_r and ε_θ, where

$$\varepsilon_r = u' + 0.5(w')^2, \quad \varepsilon_\theta = u/r. \tag{47}$$

The minimum principal stress occurs at the inner edge ($r = a$).

10.1 No radial stretching

First consider no radial stretching ($u_2 = 0$) and $\nu = 1/3$. Then the closed-form solution for $w(r)$ and $u(r)$ in Eq. (30) can be used, along with Eq. (40) for $v_e(r)$. It is found that the membrane remains taut as long as $v_1 < v_1{}^*$ where

$$v_1^* = (1 - a^2)a^{1/3}w_1^2/[27^{1/2}(1 - a^{2/3})^2]. \tag{48}$$

Therefore, for $\nu = 1/3$ and a given value of a, this threshold value $v_1{}^*$ of the torsional displacement $v_e(a)$ increases quadratically with the vertical displacement of the inner edge. The dependence of $v_1{}^*$ on the inner radius a is depicted in Fig. 12, where the quantity v_1^*/w_1^2 is plotted for the range $0 < a < 0.9$, and it is seen that the slope of the curve increases as a increases.

10.2 Outward radial stretching

Now the membrane is pulled outward with a radial deflection u_2 at the outer edge ($r = 1$), is given a downward displacement w_1 at the inner edge ($r = a$), and is then subjected to a circumferential displacement v_1 at the inner edge. For given values of ν, a, u_2, and w_1, the quantities $u'(a)$ and $w'(a)$ are varied until $u(1) = u_2$ and $w(1) = 0$. Then the value of v_1^* is computed from the resulting solution using Eq. (46).

Approximately, v_1^* increases linearly with u_2 and quadratically with w_1. In Fig. 13, $u_2 = 0.001$ and $w_1 = 0.1$, and v_1^* is plotted versus Poisson's ratio for the cases $a = 0.2$ and 0.5. Except near $\nu = 0$, v_1^* increases almost linearly with ν.

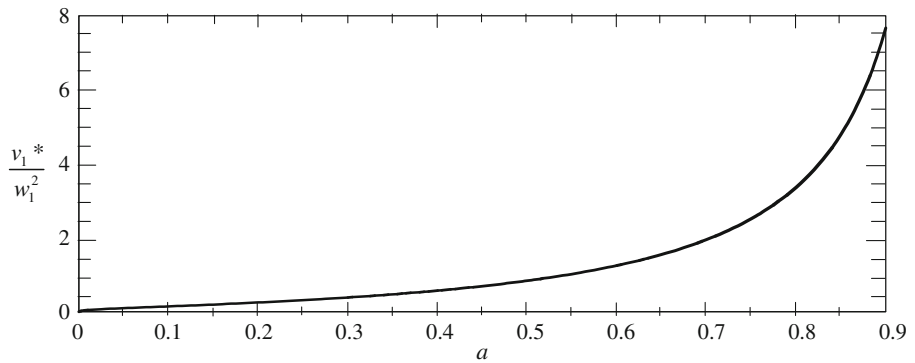

Fig. 12 Torsion and vertical displacement at inner edge: normalized threshold $v_1^*/(w_1^2)$ for wrinkling versus a; $\nu = 1/3$; no radial stretching; FvK theory

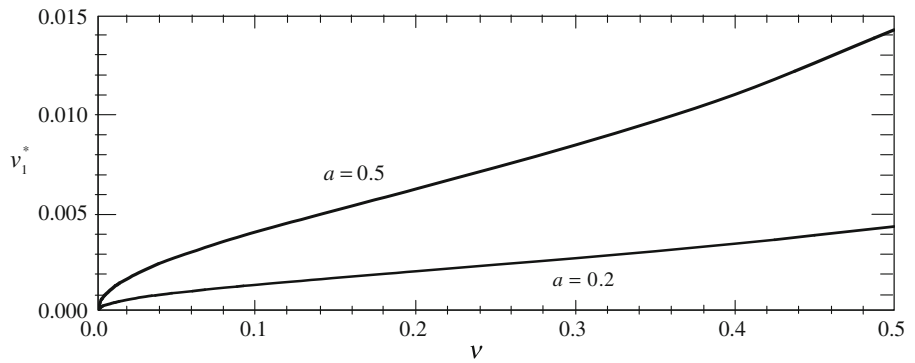

Fig. 13 Torsion and vertical displacement at inner edge: threshold v_1^* versus Poisson's ratio ν; $u_2 = 0.001$; $w_1 = 0.1$; FvK theory

11 Concluding remarks

Wrinkle-free, linearly elastic, annular and circular membranes have been considered, with coupling between transverse and stretching displacements. Rotationally symmetric equilibrium states were analyzed. Three theories were considered: the usual Föppl-von Kármán theory (FvK), Reissner's theory (R), and a new generalization of Reissner's theory (GR) that does not restrict the strains to be negligible compared to unity. The equilibrium equations were written in terms of displacements, and did not include a stress function or stresses that are used in the governing equations in many previously published studies. The forms presented in Eqs. (8)–(10), (14), (15), (21) and (22) are especially useful for the problems considered, which involve boundary conditions only on displacements, and they also are applicable when stress resultants are involved in the boundary conditions.

Displacements, strains, stress resultants, and conditions for the onset of wrinkling (when the minimum principal stress resultant reduces to zero) were obtained for a number of problems. Some of the problems considered here are apparently new, such as ponding of an annular membrane, transverse loading with a free outer edge having no slope or radial displacement, and pull-in instability of a circular or annular MEMS device in which stretching and nonuniform tension are included in the analysis. Application of the GR theory and some of the applications of the R theory are also new. In addition, a new closed-form solution was presented for a pull-off adhesion problem involving a circular membrane. In most cases, numerical solutions were required, and a shooting method was utilized to obtain them.

The discrepancies between the FvK, R, and GR results tend to increase with increasing displacements, with the R values tending to lie between the FvK and GR values. Often the displacements, strains, and stress resultants based on the GR theory have larger magnitudes than those from the FvK and R analyses.

For pulling inward (Sect. 3), wrinkling initiates at the inner edge, and the condition for wrinkling to occur depends on Poisson's ratio and the ratio of the radii of the edges of the annular edges, but not on the magnitude of the applied radial displacement at the inner edge. For torsion (Sects. 9 and 10), wrinkling also begins at the inner edge, and the threshold value of torsion for wrinkling in the FvK theory is proportional to the applied radial displacement for pulling outward, and to the square root of the applied radial displacement for pulling inward. However, for vertical loading of a horizontal annular membrane that can slide vertically but not rotate at its outer edge (Sect. 7), wrinkling begins at a circle between the inner and outer edges, and in the FvK theory the condition for wrinkling to occur does not depend on the magnitude of the load.

If a flat membrane is subjected to tension in one direction, the Poisson effect tends to cause it to be compressed and to wrinkle in the perpendicular direction [4]. This effect is more pronounced if the Poisson's ratio is higher. However, the opposite trend occurs in some of the problems studied here: wrinkling in the circumferential direction is more likely for low values of Poisson's ratio. This is due to the geometry of the annular membrane and the boundary conditions.

Since linearly elastic behavior is assumed, the GR theory will not be applicable in cases for which the material deviates significantly from such a constitutive law. However, some materials are approximately linearly elastic to strains that are not negligible compared to unity. Also, the GR theory naturally is applicable when the strains are small, and the numerical solutions for this theory may be just as easy to obtain as those for the R or FvK theories (e.g., by the shooting method utilized in this investigation).

This study has considered true membranes, with no flexural rigidity. The equations can be modified to include bending moments and shear forces, and the shooting method can again be used to obtain numerical solutions. In many physical cases the flexible structure is very thin and the behavior is dominated by stretching, with bending effects being negligible. Then the theories utilized here are applicable.

Acknowledgments This research was sponsored by the National Science Foundation under Grant No. CMS-0408281. The author is grateful to Professor George M. Filz for helpful discussions regarding Sect. 7.

References

1. Jenkins, C.H., Leonard, J.W.: Nonlinear dynamic response of membranes: state of the art. Appl. Mech. Rev. **44**, 319–328 (1991)
2. Jenkins, C.H.: Nonlinear dynamic response of membranes: state of the art—update. Appl. Mech. Rev. **49**, S41–S48 (1996)
3. Ruggiero, E.J., Inman, D.J.: Gossamer spacecraft: recent trends in design, analysis, experimentation, and control. J. Spacecr. Rockets. **43**, 10–24 (2006)
4. Cerda, E., Mahadevan, L.: Geometry and physics of wrinkling. Phys. Rev. Lett. **90**, 074302 (2003)
5. Reissner, E.: On finite deflections of circular plates. In: Non-linear problems in mechanics of continua, Proceedings of Symposia in Applied Mathematics, vol. I, pp. 213–219. American Mathematical Society, New York (1949)

6. Wolfram, S.: The Mathematica book, 3rd edn. Cambridge University Press, Cambridge (1996)
7. Plaut, R.H.: Linearly elastic annular and circular membranes under radial, transverse, and torsional loading. Part II: vibrations about deformed equilibria. Acta. Mech. doi:10.1007/s00707-008-0035-5
8. Steigmann, D.J.: Proof of a conjecture in elastic membrane theory. J. Appl. Mech. **53**, 955–956 (1986)
9. Schmidt, R., DaDeppo, D.A.: On finite axisymmetric deflections of circular plates. Z. Angew. Math. Mech. **55**, 768–769 (1975)
10. Schmidt, R., DaDeppo D., A.: On nonlinear equations governing axisymmetric deflections of circular elastic plates. J. Industrial Math. Soc. **25**(Part 2), 67–81 (1975)
11. Sukanit T.J., Peddieson J. (1981) Axisymmetric arbitrarily large deflections of circular membranes. Presented at the 18th Annual Meeting of the Society of Engineering Science, September 2–4, Brown University, Providence
12. Greschik, G., Palisoc, A., Cassapakis, C., Veal, G., Mikulas, M.M.: Sensitivity study of precision pressurized membrane reflector deformations. AIAA J. **39**, 308–314 (2001)
13. Kao, R., Perrone, N.: Large deflections of axisymmetric circular membranes. Int. J. Solids Struct. **7**, 1601–1612 (1971)
14. Lai, Y.-H., Dillard, D.A.: A study of the fracture efficiency parameter of blister tests for films and coatings. J. Adhes. Sci. Technol. **8**, 663–678 (1994)
15. Baddour, N., Zu, J.W.: A revisit of spinning disk models, Part I: derivation of equations of motion. Appl. Math. Modell. **25**, 541–559 (2001)
16. Haughton, D.M., McKay, B.A.: Wrinkling of annular disks subjected to radial displacements. Int. J. Eng. Sci. **33**, 335–350 (1995)
17. Géminard, J.-C., Bernal, R., Melo, F.: Wrinkle formations in axi-symmetrically stretched membranes. Eur. Phys. J. E. **15**, 117–126 (2004)
18. Coman, C.D., Haughton, D.M.: On some approximate methods for the tensile instabilities of thin annular plates. J. Eng. Math. **56**, 79–99 (2006)
19. Coman, C.D., Haughton, D.M.: Localized wrinkling instabilities in radially stretched annular thin films. Acta Mech. **185**, 179–200 (2006)
20. Coman, C.D.: On the applicability of tension field theory to a wrinkling instability problem. Acta Mech. **190**, 57–72 (2007)
21. Coman, C.D. Bassom A.P.: On the wrinkling of a pre-stressed annular thin film in tension. J. Mech. Phys. Solids **55**, 1601–1617 (2007)
22. Coman, C.D., Bassom, A.P.: Singular behaviour in a generalized boundary eigenvalue problem for annular plates in tension. Qtly. J. Mech. Appl. Math. **60**, 319–336 (2007)
23. Senior, B.W.: Flange wrinkling in deep-drawing operations. J. Mech. Phys. Solids **4**, 235–246 (1956)
24. Burton, K., Taylor, D.L.: Traction forces of cytokinesis measured with optically modified elastic substrata. Nature **385**, 450–454 (1997)
25. Mori, D., David, G., Humphrey, J.D., Moore, J.E.: Stress distribution in a circular membrane with a central fixation. J. Biomech. Eng. **127**, 549–553 (2005)
26. Cerda, E.: Mechanics of scars. J. Biomech. **38**, 1598–1603 (2005)
27. Nadler, B., Steigmann, D.J.: Modeling the indentation, penetration and cavitation of elastic membranes. J. Mech. Phys. Solids. **54**, 2005–2029 (2006)
28. Caldwell, L.A.: Large deflections of a thin circular membrane with a rigid inclusion. M.S. thesis, Virginia Polytechnic Institute (1968)
29. Junkin, G.: General nonlinear plate theory applied to a circular plate with large deflections. Ph.D. thesis, Virginia Polytechnic Institute (1969)
30. Tseng, C.-G., Peddieson, J.: Arbitrarily large deflections of circular membranes due to transverse loading. J. Ind. Math. Soc. **34**, 181–191 (1984)
31. Fulton, J.P., Simmonds, J.G.: Large deformations under vertical edge loads of annular membranes with various strain energy densities. Int. J. Non-Linear Mech. **21**, 257–267 (1986)
32. Tezduyar, T.E., Wheeler, L.T., Graux, L.: Finite deformation of a circular elastic membrane containing a concentric rigid inclusion. Int. J. Non-Linear Mech. **22**, 61–72 (1987)
33. Pamplona, D.C., Bevilacqua, L.: Large deformations under axial force and moment loads of initially flat annular membranes. Int. J. Non-Linear Mech. **27**, 639–650 (1992)
34. Roxburgh, D.G., Steigmann, D.J., Tait, R.J.: Azimuthal shearing and transverse deflection of an annular elastic membrane. Int. J. Eng. Sci. **33**, 27–43 (1995)
35. Libai, A., Simmonds, J.G.: The nonlinear theory of elastic shells, 2nd edn. Cambridge University Press, Cambridge (1998)
36. Foroutan-Naini, F., Peddieson, J.: Large axisymmetric deformations of elastic circular membranes. Mech. Res. Commun. **11**, 67–74 (1984)
37. Williams, J.G.: Energy release rates for the peeling of flexible membranes and the analysis of blister tests. Int. J. Frac. **87**, 265–288 (1997)
38. Wan, K.-T.: Adherence of an axisymmetric flat punch on a thin flexible membrane. J. Adhes. **75**, 369–380 (2001)
39. Wan, K.-T., Dillard, D.A.: Adhesion of a flat punch adhered to a thin pre-stressed membrane. J. Adhes. **79**, 123–140 (2003)
40. Wan, K.-T., Kogut, L.: The coupling effect of interfacial adhesion and tensile residual stress on a thin membrane adhered to a flat punch. J. Micromech. Microeng. **15**, 778–784 (2005)
41. Raegen, A.N., Dalnoki-Veress, K., Wan, K.-T., Jones, R.A.L.: Measurement of adhesion energies and Young's modulus in thin polymer films using a novel axi-symmetric peel test geometry. Eur. Phys. J. E. **19**, 453–459 (2006)
42. Ju, B.-F., Liu, K.-K., Wong, M.-F., Wan, K.-T.: A novel cylindrical punch method to characterize interfacial adhesion and residual stress of a thin polymer film. Eng. Frac. Mech. **74**, 1101–1106 (2007)
43. Plaut, R.H., White, S.A., Dillard, D.A.: Effect of work of adhesion on contact of a pressurized blister with a flat surface. Int. J. Adhes. Adhes. **23**, 207–214 (2003)
44. Allen, M.G., Senturia, S.D.: Analysis of critical debonding pressures of stressed thin films in the blister test. J. Adhes. **25**, 303–315 (1988)

45. Allen, M.G., Senturia, S.D.: Application of the island blister test for thin film adhesion measurement. J. Adhes. **29**, 219–231 (1989)
46. Liechti, K.M., Shirani, A.: Large scale yielding in blister specimens. Int. J. Frac. **67**, 21–36 (1994)
47. Jensen, H.M., Cochelin, B.: Fracture analysis of the constrained blister test. J. Adhes. **47**, 231–243 (1994)
48. Lai, Y.-H., Dillard, D.A.: An elementary plate theory prediction for strain energy release rate of the constrained blister test. J. Adhes. **31**, 177–189 (1994)
49. Hencky, H.: Über den Spannungszustand in kreisrunden Platten mit verschwindender Biegungssteifigkeit. Z. Math. Phys. **63**, 311–317 (1915)
50. Dickey, R.W.: The plane circular elastic surface under normal pressure. Arch. Ration. Mech. Anal. **26**, 219–236 (1967)
51. Peddieson, J.: Finite deflections of circular membranes. J. Eng. Mech. Div. ASCE **99**, 634–638 (1973)
52. Pai, P.F.: Highly flexible structures: Modeling, computation, and experimentation. American Institute of Aeronautics and Astronautics, Reston (2007)
53. Tuan, C.Y.: Ponding on circular membranes. Int. J. Solids Struct. **35**, 269–283 (1998)
54. Katsikadelis, J.T., Nerantzaki, M.S.: The ponding problem on elastic membranes: An analog equation solution. Comput. Mech. **28**, 122–128 (2002)
55. Smith, M.W.: Design of bridging layers in geosynthetic-reinforced column-supported embankments. Ph.D. thesis, Virginia Polytechnic Institute and State University (2005)
56. Smith, M., Filz, G.: Axisymmetric numerical modeling of a unit cell in geosynthetic-reinforced, column-supported embankments. Geosyn. Int. **14**, 1–10 (2007)
57. Pelesko, J.A., Bernstein, D.H.: Modeling MEMS and NEMS. Chapman and Hall/CRC, Boca Raton (2003)
58. Pelesko, J.A., Chen, X.Y.: Elecrostatic deflections of circular elastic membranes. J. Electrostatics **57**, 1–12 (2003)
59. Pelesko, J.A., Driscoll, T.A.: The effect of the small-aspect-ratio approximation on canonical electrostatic MEMS models. J. Eng. Math. **53**, 239–252 (2005)
60. Batra, R.C., Porfiri, M., Spinello, D.: Analysis of electrostatic MEMS using meshless local Petrov-Galerkin (MLPG) method. Eng. Anal. Bound. Elem. **30**, 949–962 (2006)
61. Batra, R.C., Porfiri, M., Spinello, D.: Effects of Casimir force on pull-in instability in micromembranes. EPL **77**, 20010 (2007)
62. Ghoussoub, N., Guo, Y.: On the partial differential equations of electrostatic MEMS devices: stationary case. SIAM J. Math. Anal. **38**, 1423–1449 (2007)
63. Saif, M.T.A., Alaca, B.E., Sehitoglu, H.: Analytical modeling of electrostatic membrane actuator for micro pumps. IEEE J. Microelectromech. Sys. **8**, 335–345 (1999)
64. Faris, W.F.: Nonlinear dynamics of annular and circular plates under thermal and electrical loadings. Ph.D. thesis, Virginia Polytechnic Institute and State University (2003)
65. Duan, G., Wan, K.-T.: Analysis of one-dimensional and two-dimensional thin film "pull-in" phenomena under the influence of an electrostatic potential. J. Appl. Mech. **74**, 927–934 (2007)
66. Reissner, E.: On tension field theory. In: Den Hartog, J.P., Peters, H. (eds.) Proceedings of the 5th International Congress of Applied Mechanics. Wiley, New York, pp. 88–92 (1939)
67. Stein, M., Hedgepeth, J.M.: Analysis of partly wrinkled membranes. NASA Technical Note D-813, National Aeronautics and Space Administration, Washington, DC (1961)
68. Mikulas, M.M.: Behavior of a flat stretched membrane wrinkled by the rotation of an attached hub. M.S. thesis, Virginia Polytechnic Institute (1964). Also NASA TN D-2456 (1964)
69. Roddeman, D.G.: Finite element analysis of wrinkling membranes. Comm. Appl. Num. Meth. **7**, 299–307 (1991)
70. Li, X., Steigmann, D.J.: Finite plane twist of an annular membrane. Quarterly J. Mech. Appl. Math. **46**, 601–625 (1993)
71. Kang, S., Im, S.: Finite element analysis of wrinkling membranes. J. Appl. Mech. **64**, 263–269 (1997)
72. Adler, A.L., Mikulas, M.M., Hedgepeth J.M.: Static and dynamic analysis of partially wrinkled membrane structures. In: 41st AIAA/ASME/ASCE/AHS/ASC structures, structural dynamics, and materials conference and exhibit, paper AIAA-2000–1810, Atlanta (2000)
73. Miyamura, T.: Wrinkling on stretched circular membrane under in-plane torsion: Bifurcation analyses and experiments. Eng. Struct. **22**, 1407–1425 (2000)
74. Lu, K., Accorsi, M., Leonard, J.: Finite element analysis of membrane wrinkling. Int. J. Num. Meth. Eng. **50**, 1017–1038 (2001)
75. Schoop, H., Taenzer, L., Hornig, J. : Wrinkling of nonlinear membranes. Comput. Mech. **29**, 68–74 (2002)
76. Ding, H., Yang, B., Lou, M., Fang, H.: New numerical method for two-dimensional partially wrinkled membranes. AIAA J. **41**, 125–132 (2003)
77. Iwasa, T., Natori, M.C., Higuchi, K.: Evaluation of tension field theory for wrinkling analysis with respect to the post-buckling study. J. Appl. Mech. **71**, 532–540 (2004)
78. Nakashino, K., Natori, M.C.: Efficient modification scheme of stress–strain tensor for wrinkled membranes. AIAA J. **43**, 206–215 (2005)
79. Rossi, R., Lazzari, M., Vitaliani, R., Oñate, E.: Simulation of light-weight membrane structures by wrinkling model. Int. J. Num. Meth. Eng. **62**, 2127–2153 (2005)
80. Hossain, N.M.A., Jenkins, C.H., Woo, K., Igawa, H.: Transverse vibration analysis for partly wrinkled membranes. J. Spacecr. Rockets **43**, 626–637 (2006)
81. Jenkins, C.H.M., Hossain, N.M.A., Woo, K., Igawa, H., Wang, J.T., Sleight, D.W., Tessler, A.: Membrane wrinkling. In: Jenkins, C. H. M. (ed.) Recent advances in Gossamer spacecraft, pp. 109–163, AIAA, Reston (2006)
82. Lee, E.-S., Youn, D.-S., S.-K.: Finite element analysis of wrinkling membrane structures with large deformation. Finite Elem. Anal. Des. **42**, 780–791 (2006)
83. Miyazaki, Y.: Wrinkle/slack model and finite element dynamics of membrane. Int. J. Num. Meth. Eng. **66**, 1179–1209 (2006)
84. Akita, T., Nakashino, K., Natori, M.C., Park, K.C.: A simple computer implementation of membrane wrinkle behaviour via a projection technique. Int. J. Num. Meth. Eng. **71**, 1231–1259 (2007)

85. Coman, C.D., Bassom, A.P.: Boundary layers and stress concentration in the circular shearing of annular thin films. Proc. R. Soc. Lond. A. **463**, 3037–3053 (2007)
86. Coman, C.D., Bassom, A.P.: Wrinkling of pre-stressed annular thin films under azimuthal shearing. Math. Mech. Solids **13**, (2008) (to appear)
87. Shaw, A., Roy, D.: Analyses of wrinkled and slack membranes through an error reproducing mesh-free method. Int. J. Solids Struct. **44**, 3939–3972 (2007)
88. Chia, C.-Y.: Nonlinear analysis of plates. McGraw-Hill, New York (1980)